2.5 TEM OBSERVATION OF ANNEALED AND He IMPLANTED NANOSTRUCTURED FERRITIC ALLOYS—Y. Wu, T. Stan, T. Yamamoto, G. R. Odette (University of California Santa Barbara)

OBJECTIVE

The objective of this study is to characterize the details of He bubble association with Y-Ti-O oxides in nanostructured ferritic alloys (NFAs).

SUMMARY

Transmission electron microscopy (TEM) studies were carried out on two 700°C He implanted NFAs that had been previously annealed to coarsen their initially ultra-high density of nano-scale oxides (NOs). All the coarsened Y-Ti-O oxides were found to be associated with at least one, and in many cases more than one, interface helium bubble.

PROGRESS AND STATUS

Introduction

Managing helium is a grand challenge for turning the promise of C-free fusion power into a reality. Nanostructured ferritic alloys (NFAs), promising candidates for fusion applications, are dispersion strengthened by an ultrahigh density ($\approx$ 5 x $10^{23}/m^3$) of Y-Ti-O nano-scale ($\approx$ 2.5 nm) oxides (NOs) with volume fractions of $\approx$ 0.5% for MA957 [1-3]. NOs trap otherwise highly damaging helium in harmless nm-scale interface bubbles [1-3], and thus they effectively manage very high concentrations of this insoluble transmutation product formed in fusion reactor materials. Hence, understanding the mechanisms of bubble formation, and bubble association with NOs, is essential to developing, qualifying and optimizing NFAs. However, when the NOs are very small, it is more difficult to characterize both the bubbles and their detailed oxide associations. Thus high temperature annealing was used to coarsen the oxides up to much larger sizes. The annealed NFAs were then implanted to a peak concentration of 4100 appm He at 700°C to form a population of bubbles on the coarsened oxides.

The ultimate objective of this study is to carry out detailed characterization of a He implanted NFA microstructure at the Lawrence Berkeley Laboratory (LBL) National Center for Electron Microscopy (NCEM), using their FEI Titan TEAM 1 and/or TEAM 0.5 aberration corrected TEMs. Here we briefly describe a preliminary scoping study carried out on the UCSB FEI Titan TEM. Four annealed and He implanted NFA MA957 FIBed lamella lift-outs were examined, and 2 lift-outs from another 14YWT NFA were characterized.

Materials

TEM studies were carried out on annealed NFA MA957 and a 14YWT developmental heat called V540H. V540H was powder processed by ball milling atomized powders to dissolve phase separated Y and consolidated by HIPing at 1150°C. Details about these alloys can be found elsewhere [4-6]. The as extruded MA957 was annealed at 1200°C for 2000 h. A calibrated coarsening model was used to estimate the average NO diameter of <d> $\approx$ 9 – 10 nm. The 14YWT sample was annealed at 1200°C for 228 hrs, with an estimated NO diameter of <d> $\approx$ 6 – 7 nm.

The annealed alloys were single He-ion (1 MeV) implanted at 700°C at the Kyoto University DuET facility in Japan at a dose rate of 1.2 x 10^{12} He/cm^2/s. A spinning degrader foil was used to spread out the He implantation profile, which is shown as a red solid curve in Figure 1. TEM examinations were carried out over the full $\approx$ 1.5 µm implanted region. The peak He concentration is 4100 appm at a depth of ~ 1.2 µm.

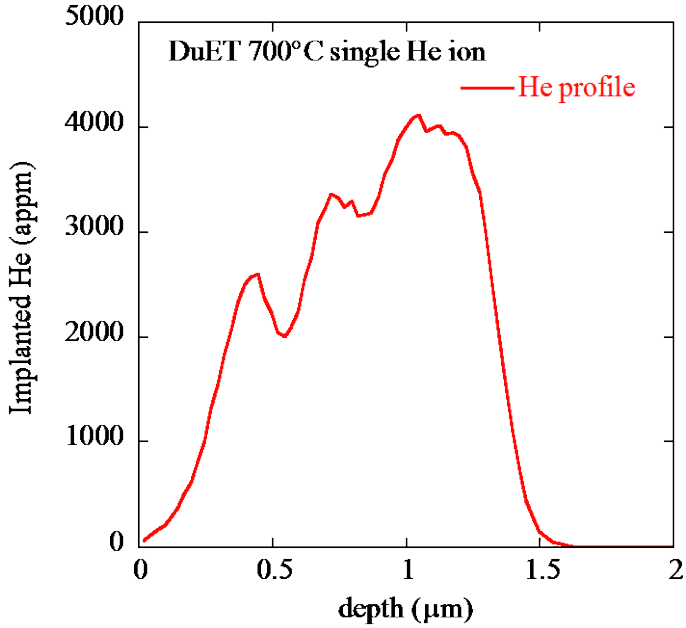

Figure 1. SRIM imulation of the He implantation profile in the MA957 and V540H NFA.

FIB lift-out electron transparent TEM lamella was prepared on a FEI Helios dual beam SEM. A finial 2 kV, 5.5 pA low energy ion beam was used to minimize gallium damage. Bright field (BF), scanning transmission electron microscopy (STEM) and high resolution electron microscopy (HRTEM) were used to observe the implanted microstructures. STEM was used to determine the number density (N), average diameter (<d>) and volume fraction (f) of the NOs and bubbles, while HRTEM Fast Forier Transform (FFT) indexing was used to study the NO crystal structure. The data was collected at 300 kV on a FEI Titan and recorded on a 2048 x 2048 pixel CCD camera. The HRTEM images were analyzed by FFT power spectrum indexing. The lattice spacings and inter-planar angles were measured using ImageJ.

Results

Previously, TEM showed that the unannealed V540H contained N_p = 6.5 x $10^{23}/m^3$, $<d_p>$ = 1.5 nm NOs with f_p = 0.18%. Small angle neutron scattering (SANS), atom probe tomography (APT) and TEM results on V540 powders annealed to simulate the HIP temperature cycle, found an average of N_p = 6.2 x $10^{23}/m^3$, $<d_p>$ = 1.7 nm NOs with f_p = 0.52%. The corresponding results of more comprehensive studies of MA957 showed that N_p = 5.0 x $10^{23}/m^3$, $<d_p>$ = 2.5 nm NOs with f_p = 0.50%.

Representative low magnification STEM images of He implanted annealed MA957 and V540H are shown in Figure 2. The oxides and cavities image in STEM as the lighter and darker features, respectively. The average coarsened NO $<d_p>$ are $\approx$ 40.4 nm in MA957 and 8.2 nm in V540H. The corresponding NO N_p are $\approx$ 5.9 x $10^{20}/m^3$ and $\approx$ 6.3 x $10^{21}/m^3$, while the corresponding f_p are $\approx$ 2.9% and 0.27%, respectively. Clearly, the NO coarsened (increased $<r_p>$ and decreased N_p) significantly after annealing in both cases. The NO f_p in V540H did not change much after annealing, while apparently the f_p increased enormously in the case of MA957.

Figure 3 shows bubbles on the NO interfaces. The cavity sides and faces are clearly faceted when not attached to NOs, while the faces that are attached to the NOs are not clearly seen in Figure 3 due to the imaging direction. In both annealed NFAs, all of the oxides are associated with at least one, and many cases more than one interface He bubble. The corresponding average bubble diameters, $<d_b>$, are $\approx$ 32.5 nm and $\approx$ 6.3 nm while the N_b are $\approx$ 6.4 x $10^{20}/m^3$ and $\approx$ 6.8 x $10^{21}/m^3$ for MA957 and V540H, respectively. The corresponding f_b are $\approx$ 2.3% and 0.10%.

Figure 4 shows a HRTEM image (a) and the corresponding FFT power spectrum (b) for a ≈ 4 x 6 nm oxide in 14YWT. After excluding multiple diffraction spots, the FFT diffraction pattern in Figure 2b has d-spacings and inter-planar angle, shown in Table 1, that are consistent with the same NO $Y_2Ti_2O_7$ pyrochlore crystal structure in the unannealed and unimplanted condition [4,6]. Further, the orientation relationship between this precipitate and ferrite matrix is cube-on-edge: [100] with a $[100]_{YTO}$ || $[010]_{Fe}$ and $[011]_{YTO}$ || $[100]_{Fe}$, as found by Dawson et al. [7], Ribis et al. [8] and Wu et al. [9].

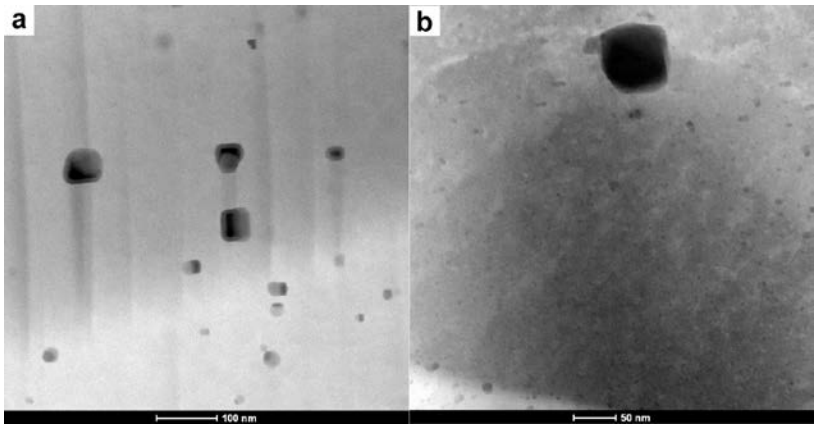

Figure 2. Low magnification STEM images of: a) annealed MA957 showing faceted cavities and coarsened oxide precipitates with a wide distribution of sizes; and, b) annealed 14YWT showing much smaller and more numerous associated bubbels and precipitates, that includes one very large cavity.

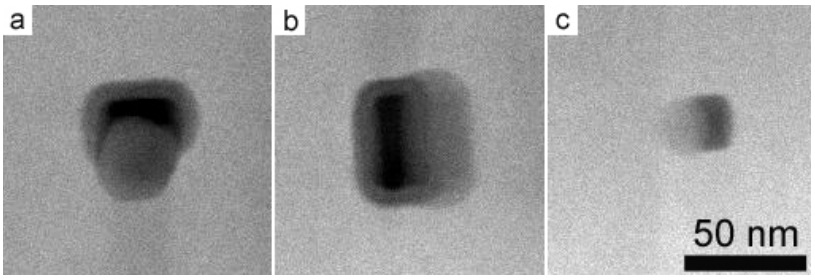

Figure 3. Higher magnification STEM images of annealed MA957, showing cavities attached to the NOs.

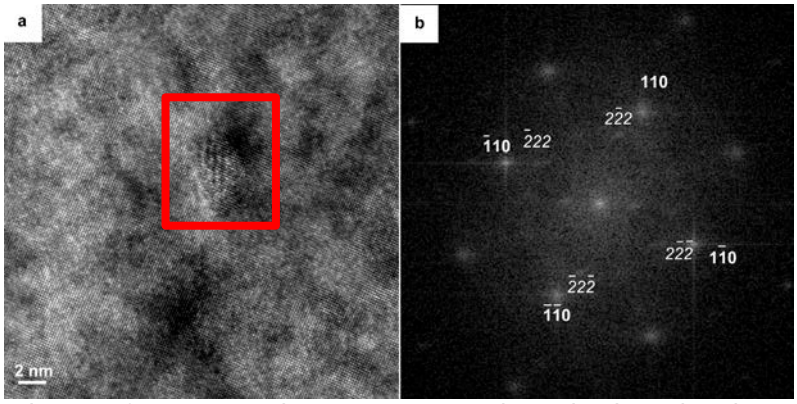

Figure 4. a) HRTEM image of a coarsened 4 nm x 6 nm NO in He implanted and annealed 14YWT; and, b) the corresponding FFT power spectrum.

Table 1. The measured d-spacings and plane angle from Fig. 2b compared to those for bulk $Y_2Ti_2O_7$.

Alloy	**d (Å)**	**d_1(2-22)**	**d_2(22-2)**	**α_{12}(°)**
V540H	Measured	2.83±0.09	2.83±0.09	72.2±0.9
	$Y_2Ti_2O_7$	2.90	2.90	70.5

Figure 5 shows a HRTEM image (a) of a large cuboidal 28 x 24 nm oxide from the annealed MA 957 and (b) corresponding FFT power spectra. In this case the d-spacings and inter-planar angle, shown in Table 2, are not consistent with $Y_2Ti_2O_7$, or any other known Y-Ti-O phase.

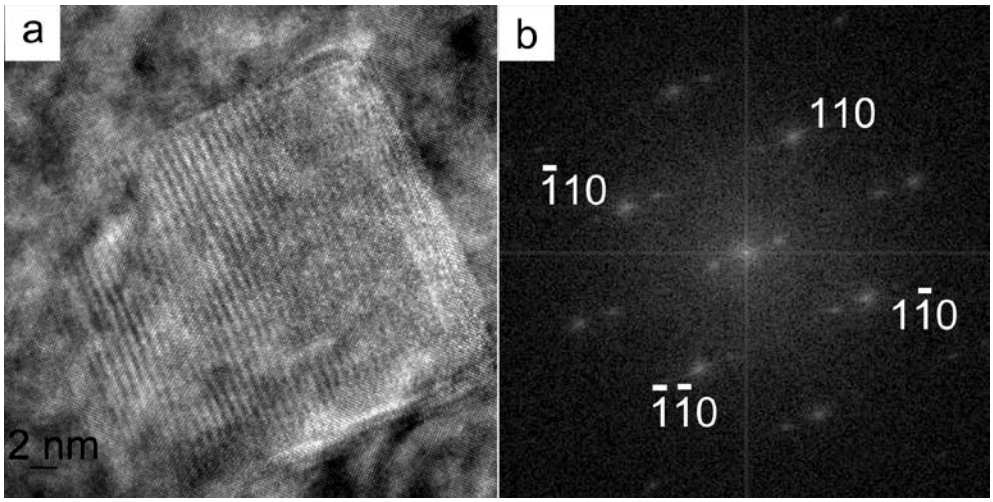

Figure 5. a) HRTEM image of a 28 x 24 nm coarsened oxide in annealed and He implanted 14YWT; and, b) the corresponding FFT power spectrum.

Table 2. The measured d-spacings and inter-planar angle in annealed MA957.

Alloy	**d (Å)**	**d_1**	**d_2**	**α_{12}(°)**
MA 957	Measured	2.45±0.09	2.45±0.09	65.0±0.9

Discussion

Detailed analysis of these results will be carried out after additional characterization at UCSB and LBL - NCEM. However, tentative preliminary conclusions include:

- Annealing coarsens the NOs in both NFA and in MA957. A large amount of additional oxide precipitation is observed.
- Even with much lower N and sink densities compared to the unannealed condition, the much larger oxides in the annealed MA957 collect a large fraction of the implanted He, which resides in very large attached interface bubbles.
- The smaller, but still coarsened, NO in annealed V540H are associated with much smaller interface bubbles.
- The NO and bubbles are similar to those in the annealed V540H, but even smaller in the unannealed MA957 and a 14YWT NFA called PM2, that is generally similar to V540H.

- In all cases (annealed and unannealed) all of the oxides are associated with one or more bubbles.

Future Work

The first set of measurements on the He implanted NFAs the LBL NCEM is scheduled for Sept. 26 – 29, based on a successful user proposal. TEM at UCSB will continue both before and after the visit.

Acknowledgements

Research at UCSB was supported by the Department of Energy Office of Fusion Energy Sciences (Grant No. DE-FG03-94ER54275) and the development of V540H was Office of Nuclear Energy (Grant No. DE-FC07-07ID14825). TEM specimen preparation and measurements were carried out in the UCSB Materials Research Laboratory Microstructure and Microanalysis Facility, supported by the Materials Research Science and Engineering Center Program of the National Science Foundation under Award No. DMR05-20415.

References

[1] G. R. Odette, M. J. Alinger, and B. D. Wirth, *Annu. Rev. Mater. Res*. 38 (2008) 471-503.
[2] G. R. Odette, *JOM* 66 (2014) 24272441.
[3] Y. Dai, G. R. Odette, and T. Yamamoto, *Comp. Nuc. Mater.* 1 - Chap 6, Elsevier 141 (2012).
[4] Y. Wu, E. Haney, N. Cunningham, G. R. Odette, *Acta Mater*. 60 (2012) 3456-3468.
[5] N. J. Cunningham, Ph.D. Thesis, University of California, Santa Barbara, Santa Barbara CA (2012).
[6] N. J. Cunningham, Y. Wu, G. R. Odette, et al. Fusion Materials Semiannual Progress Report, DOE/ER- 0313/53 (2012).
[7] K. Dawson, and G. J. Tatlock, *J. Nucl. Mater.* 444 (2014) 252-260.
[8] J. Ribis, Y. DeCarlan, et al., J. Mater. Res. 30 (2015) 2210-2221.
[9] Y. Wu, J. Ciston, S. Kraemer, et al. *Acta Mater*. 111 (2016) 108-115.